GEOGRAPHICAL REPORTS
OF TOKYO METROPOLITAN UNIVERSITY 46 (2011) 13-30

DETECTION OF THE ATMOSPHERIC PRESSURE DEPRESSION IN THE CENTER OF TOKYO USING DATA CORRECTED BY ASSUMING HYDROSTATIC EQUILIBRIUM: A CASE STUDY WHEN A TYPICAL URBAN HEAT ISLAND EXISTED IN THE CENTER OF TOKYO AT NIGHTTIME SUMMER

Kazuyuki TAKAHASHI[*], Hideo TAKAHASHI

and Takehiko MIKAMI[**]

Abstract The present study represents the first ever investigation of the atmospheric pressure distribution in the Tokyo ward area at nighttime in summer using observational data. Data were sourced from Tokyo's high density Metropolitan Environmental Temperature and Rainfall Observation System (METROS). The METROS data required correction in order to determine the detailed pressure distribution in the city, due to the instrument errors specific to each station. Since the METROS observational instruments had already been removed, we corrected the atmospheric pressure data using measured pressure differences between the Tokyo Meteorological Observatory and each METROS station, at a time when the temperature at each METROS station was equal to that at the Tokyo Meteorological Observatory, based on temperature measurements under hydrostatic equilibrium conditions. The corrected pressure distribution calculated in this study was found to be reasonable because it was spatially consistent with the air temperature distribution, wind system, and convergence zone. In a case study when a typical urban heat island existed in the center of Tokyo, we detected a significant atmospheric pressure decrease of 0.2 or 0.3 hPa in the center of Tokyo compared to surrounding areas.

Key words: urban heat island, atmospheric pressure depression, pressure data correction, hydrostatic equilibrium, Tokyo

[*] Tokyo Metropolitan Research Institute for Environmental Protection.

[**] Faculty of Liberal Arts, Teikyo University.

1. Introduction

Wind convergence toward the center of a city from the suburbs is one characteristic of an urban heat island (hereafter referred to as "UHI"; e.g., Landsberg 1981; Oke 1987). There have been a large number of studies on the relationship between UHIs and wind convergence over many years (Okita 1960; Chandler 1965; Bornstein and Johnson 1977; Shreffler 1978, 1979; Fujibe and Asai 1980; Fujibe 1988, 2003; Childs and Raman 2005). However, the magnitude of the pressure depression within a city that causes wind convergence is minute. Since no observational network capable of detecting this pressure depression with high accuracy and density has been available, the relationship between pressure and wind convergence has not previously been analyzed directly.

For this reason, various methods have been employed to establish the relationship between temperature rise and pressure depression in a city. Fujibe (1987) estimated the urban boundary layer height (the height up to which the high temperature of a city exerts an influence) from the temperature and pressure differences between weekdays and weekends using 25 years of data. Also, Fujibe (1994) examined the relationship between the pressure depression and the change in the heat content of the lower atmospheric layer above the Kanto Plain over a 30 year period, and showed how these factors related to an extensive temperature rise in the metropolitan area. Sawada and Takahashi (2007) estimated the relative pressure depression in Tokyo by applying the temperature differences between Tokyo and Choshi, or Tsujido to the hydrostatic equilibrium equation, and compared the results to observational data. These previous studies analyzed the relationship between the temperature rise and the pressure depression in a city. However, they were not able to show the atmospheric pressure distribution inside a city, instead focusing on the long-term trend in pressure depression, or indirectly estimating the magnitude of the pressure depression at a specific point.

Concern over weather phenomena inside cities, such as the UHI phenomenon and convective precipitation, is increasing. Detailed meteorological observations including atmospheric pressure measurements, which can provide important information, have been carried out by some municipalities and meteorological companies, including the Metropolitan Environmental Temperature and Rainfall Observation System (METROS). The METROS observation network was installed by the Tokyo Metropolitan Research Institute for Environmental Protection (TMRIEP) in order to identify the actual state of the UHI in the center of Tokyo. Observations were performed through the collaboration of TMRIEP and the Laboratory of Climatology of Tokyo Metropolitan University. METROS observed atmospheric pressure as well as air temperature, relative humidity, wind direction, and wind speed. Analysis of the atmospheric pressure distribution in Tokyo should therefore be possible using METROS data.

Although Nishina and Mikami (2008) analyzed the diurnal change in atmospheric pressure in the Tokyo ward area using METROS data, their study suggested that the distribution of sea level pressure included instrument errors specific to each station. The present study also confirms the presence of instrument errors, and these must be corrected to determine the detailed pressure distribution inside Tokyo.

Correction of the error associated with a specific barometer is commonly carried out by comparison with a standard barometer, as described in the Japanese Meteorological Agency

(JMA 2002), if the barometer to be corrected is still present. However, the METROS observational instruments had already been removed, so correction using this method is impossible.

This study instead attempts to calculate instrument errors within the pressure data under calm conditions at nighttime by assuming that hydrostatic equilibrium conditions existed. Under such conditions, temperature can be used as a direct indicator of pressure. Therefore, choosing a time when the temperature at each METROS station was the same as that at a JMA reference station in central Tokyo (hereafter referred to as "Otemachi"), the measured pressure differences between the METROS station and Otemachi can be taken as the instrument errors and used to correct the pressure distribution data. In this way, this study aims to determine the detailed pressure distribution in the Tokyo ward area, and to detect the pressure depression in the center of Tokyo due to the UHI at nighttime.

2. Method for Correction of Atmospheric Pressure Data

Equation (1) is obtained by integrating the hydrostatic equilibrium equation vertically, and represents the relationship between the temperature difference ΔT of two stations and the pressure difference Δp of two stations up to a height H.

$$\Delta p = g\int_0^H \Delta\rho dz = -\frac{\rho_0 g}{T_0}\int_0^H \Delta T dz \qquad (1)$$

Here, g is the gravitational acceleration (9.81 ms^{-2}), T_0 is the standard temperature of 298 K (25 °C), ρ_0 is the air density at this temperature (1.184 kgm^{-3}), and H is the height of the urban boundary layer (the height up to which the UHI exerts an influence).

Supposing a horizontal extent as large as a city (about 30 km × 30 km), and assuming that there is no horizontal air temperature difference above H, then there is no horizontal pressure difference at height H. If the temperature difference between two stations is ΔT up to height H, the pressure difference Δp between the two stations is represented by Eq. (1).

According to Eq. (1), if the influence of synoptic or local pressure gradients is negligible, and if the boundary layer height and the vertical distribution of temperature are equal, then the sea level pressures at stations with equal surface air temperatures can be considered to be the same. Thus, this study focuses on stable nighttime conditions when the horizontal synoptic pressure gradients are small. When the surface air temperature at each METROS station equals that at Otemachi, this study identifies the difference between the measured value on the barometer at each METROS station and the pressure at Otemachi under these calm conditions as the instrument error.

On the other hand, the height of the urban boundary layer and the vertical distribution of air temperature are thought to change with time, and also by station's location. Oke (1987) observed the vertical temperature distribution when a typical UHI occurred close to sunrise, and found that the urban boundary layer had a dome shape that was high in the center and low in the surrounding areas.

The height of the urban boundary layer over surrounding areas is generally said to be lower than that over the central area.

However, this study focuses on the METROS network mainly within the Tokyo ward area, which is influenced by the UHI in the center of Tokyo. Also, since atmospheric pressure differences from Otemachi are measured only when the temperature at each METROS station is the same as that at Otemachi, proportionate development of the urban boundary layer can be assumed in surrounding areas. For this reason, the assumption that the height of the urban boundary layer is uniform is considered reasonable. Also, when the surface air temperature at each METROS station and that at Otemachi are equal, it can be assumed that the vertical temperature distribution over each METROS station and that over Otemachi is the same because the vertical temperature distribution in the urban boundary layer becomes the distribution based on iso-potential temperature. Moreover, by averaging many similar examples, the difference associated with a particular example or time variation is removed, and the typical state at nighttime is obtained.

Furthermore, the pressure measured by a barometer is affected by the instrument error, temperature, gravitational acceleration and kinetic wind pressure (JMA 2002). However, electrostatic capacity type barometers have already been compensated for temperature using the observed air temperature, and for gravitational acceleration using the known latitude and longitude of the observation station (JMA 2002). The METROS barometer was also an electrostatic capacity type. So, this method based on measuring pressure differences under calm conditions therefore targets the instrument error alone.

3. Method

Data

In addition to METROS data, data from the JMA around the Kanto area were used in this study.

The arrangement of the METROS observation stations is shown in Fig. 1 (b). METROS comprised two meteorological observation systems: METROS20 and METROS100. The main purpose of METROS20 systems was to observe wind speed and direction above the urban canopy layer; therefore, these systems were installed on the rooftops of 20 high-rise buildings. The sea level atmospheric pressure of METROS20 was calculated by the METROS20 systems from the observed atmospheric pressure, the observed air temperature, and the altitude at an observation point using the same conversion equation and the same parameters expressed in JMA (2002). The conversion method of the METROS20 pressure data is the same as that of the Otemachi data, so we can compare them directly.

METROS100 systems, on the other hand, were used to perform detailed measurements of the temperature distribution. METROS100 systems comprised automatic recording thermometers, which were installed in the instrument shelters of 100 (106 since April 2003) elementary schools with an approximate spatial density of one station in each 2.5 km × 2.5 km area.

The JMA observatory at Otemachi was selected as a standard for temperature and pressure data against which the METROS20 data was corrected. The data from other observatories were used to select days when synoptic pressure gradients were small, allowing correction of the METROS20 data. The location of the four stations (Niigata, Tsuruga, Choshi, and Ajiro) used to calculate the synoptic

pressure gradients are shown in Fig. 1 (a). Table 1 shows the observation elements, units, and intervals of the METROS, JMA observatory, and AMeDAS data used in the present study.

Table 1 The observation elements, units, and intervals of the METROS, JMA observatory, and AMeDAS data used in the present study

Data Source	Temperature Accuracy	Wind Direction	Wind Speed	Other Parameters	Time Interval
METROS20	0.1°C	16 points of compass	0.1 m/s	Pressure, Rainfall, etc.	10 min
METROS100	0.1°C	—	—	Humidity	10 min
Observatory of JMA	0.1°C	16 points of compass	0.1 m/s	Pressure, Rainfall, etc.	1 hour
AMeDAS of JMA	0.1°C	16 points of compass	1 m/s	Rainfall, Daylight hours, etc.	1 hour

Time period of analysis

As described in Section 2, the atmospheric pressure data are corrected assuming that if air temperatures are equal then pressures are also equal under hydrostatic equilibrium. This assumption is thought to hold when the surrounding pressure gradient is small.

Therefore, this study focused on the period from July to August. During this period, there must have been many days when the synoptic pressure gradient is small, as the main island of Japan is widely covered by a Pacific High. Also, as annual trends could be included in the METROS20 atmospheric pressure data, a single year with as much data as possible in the period from July to August was selected.

Continuous data during July and August are available for 2003 and 2004. However, 2003 had many cloudy and rainy days due to a cool summer (MSJ 2003), and there were few days when the pressure gradient was small due to the existence of a low pressure and a front. In comparison, 2004 had many fine days during a hot summer, and Japan was widely covered with a Pacific High (MSJ 2004), resulting in many days when the pressure gradient was small. For these reasons, this study focuses on the period from July to August 2004.

Next, we selected days when the pressure gradient was small so that hydrostatic equilibrium could be assumed, allowing correcting of the pressure data. The measurement interval of the METROS20 barometer was 0.1 hPa. Moreover, the area covered by the METROS20 network is a maximum of about 30 km in the E-W direction. We selected days when the atmospheric pressure gradient was less than 0.3 hPa/100 km, corresponding to a pressure difference after correction of less than 0.1 hPa over the whole METROS20 area. The pressure gradient was calculated from pressure differences in the N-S and E-W directions using the daily averaged sea level pressures at four JMA observatories around the Kanto area (Fig. 1a). All four stations were coastal stations since atmospheric pressure data from inland observatories must have been influenced by local thermal highs and lows generated in the central mountainous area (Takahashi 1998). Pressure differences in the N-S direction were calculated from Ajiro (35°02.7′N, 139°05.5′E) to Niigata (37°54.7′N, 139°02.8′E), which lie at almost the same longitude, and pressure differences in the E-W direction were calculated from Choshi (35°44.3′N,

140°51.4′E) to Tsuruga (35°39.2′N, 136°03.7′E), which lie at almost the same latitude, and pressure gradients were then calculated in units of hPa per 100 km. These pressure gradients were composed into vectors, and days when the pressure gradients were less than 0.3 hPa/100 km were selected (hereafter referred to as "weak pressure gradient days"); 12 such days were selected during the months of July and August 2004.

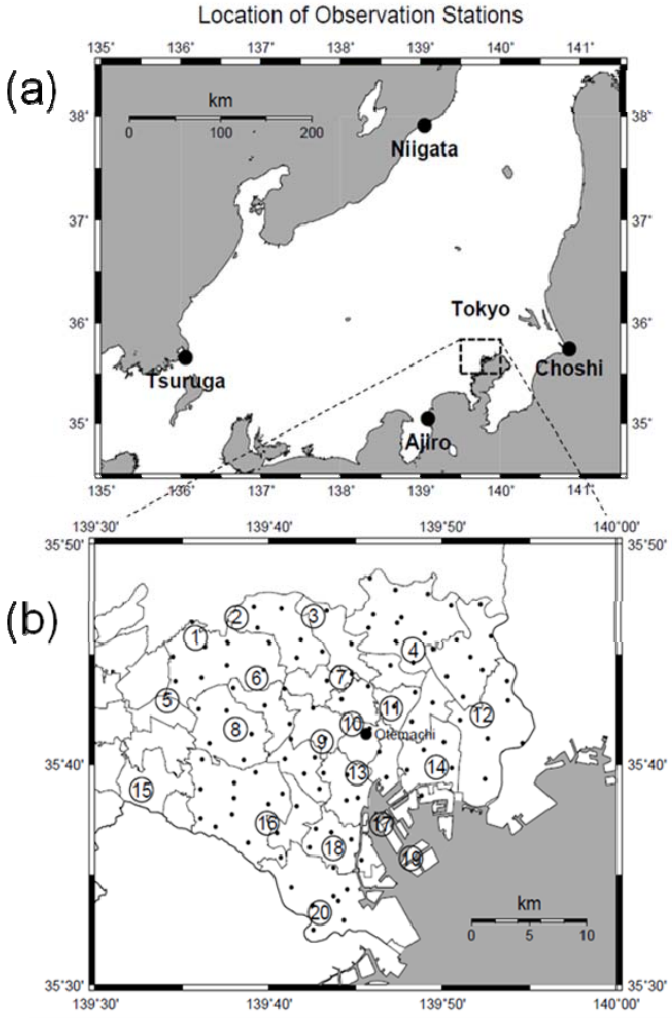

Fig. 1 (a) Location of all observation stations used in this study. (b) Arrangement of the METROS stations in Tokyo. The circled numbers are METROS20 and the dots are METROS100 stations.

Moreover, even if the synoptic pressure gradient is small, local pressure gradients that give rise to daytime sea breezes are usually present. In the coastal area of Tokyo in summer, southerly winds continue blowing until midnight in many cases (Mikami 2006). For this reason, this study targeted the time period from 00:00 to 07:00, after southerly winds become weaker and before the inherent sea breezes begin to blow.

Procedure of pressure data correction

As described in the previous section, it is possible to correct pressure data when the surface air temperatures at a given METROS20 station and that at Otemachi are equal. The temperature at Otemachi was observed at 1.5 m above the ground surface while temperatures at METROS20 were observed at various heights from 27 to 193 m, so that METROS20 temperatures must be converted to surface air temperatures. Although a temperature lapse rate is sometimes used to convert air temperature, this study used the METROS100 surface air temperature data because of its high spatial density. However, since the spatial locations of the METROS100 stations are different from those of the METROS20 stations, the METROS100 data could not be used directly.

Instead, the surface air temperatures at METROS20 stations were estimated by interpolating the METROS100 data, and pressure differences were measured when they were equal to the temperature at Otemachi in accordance with the procedure shown in Fig. 2. The subscript (n) of each variable means the station number of METROS20 stations.

To the beginning, the temperature data observed at METRO100 are spatially interpolated using the surface algorithm of "The Generic Mapping Tools (GMT4.3.1)," which is a mapping program (Wessel and Smith 1998), and the surface air temperatures tE(n) at all METROS20 stations are estimated. Then, the estimated surface air temperatures tE(n) and the observed temperatures t(n) of METROS20 are compared, and the temperature correction values c(n) at all METROS20 stations are

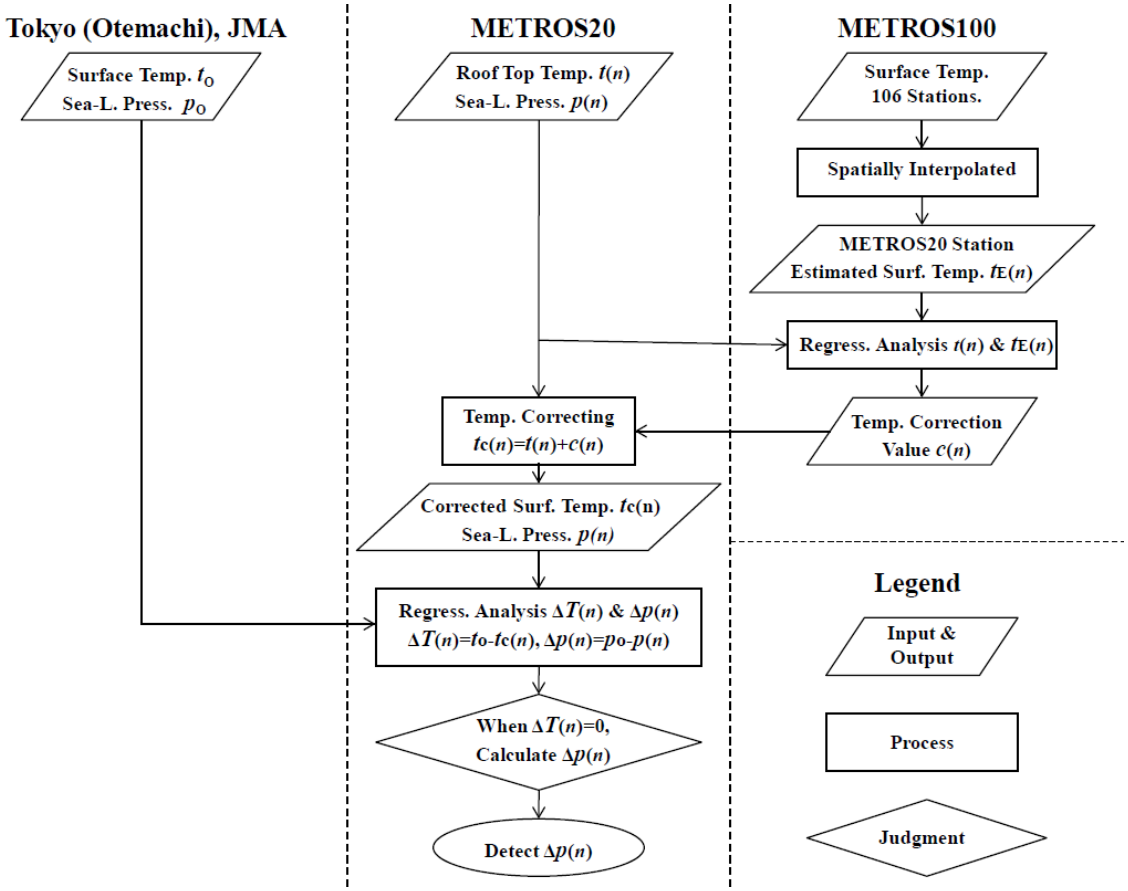

Fig. 2 Flow diagram for correcting METROS20 temperature and detecting pressure difference Δp. The subscript (n) of each variable means the station number of METROS20 stations.

obtained (see the second section of Chapter 4). Finally, the corrected surface air temperature $tc(n)$ at each METROS20 station is obtained, and the difference $\Delta p(n)$ between the sea level atmospheric pressures is calculated when the corrected surface air temperature $tc(n)$ at each METROS20 station is equal to the surface air temperature to at Otemachi.

4. Results and Discussion

Characteristic of METROS20 atmospheric pressure data

Figures 3 and 4 show uncorrected sea level pressure and wind vector distributions at 02:00 and 07:00 JST, respectively, on July 8, 2004, which was a weak pressure gradient day (pressure gradient = 0.28 hPa/100 km). The pressure is shown as a deviation from the pressure at Otemachi. The interval of the isobars is 0.1 hPa, and the broken lines indicate negative deviations. A number of inconsistencies are present in Fig. 3 and Fig. 4. Low pressure regions appear in the northern area and near Station 18 regardless of time, and a similar characteristic pressure distribution pattern to that reported by Nishina and Mikami (2008) is seen. Although the pressure gradient in the northern area would produce a

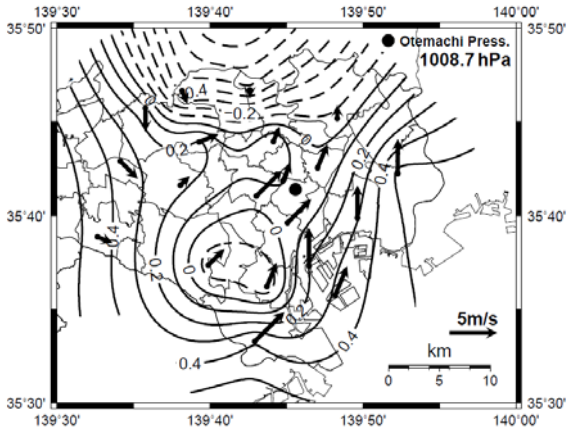

Fig. 3 Uncorrected sea level pressure distribution (deviation from Otemachi) of METROS20 and wind vectors at 02:00 JST July 8, 2004.

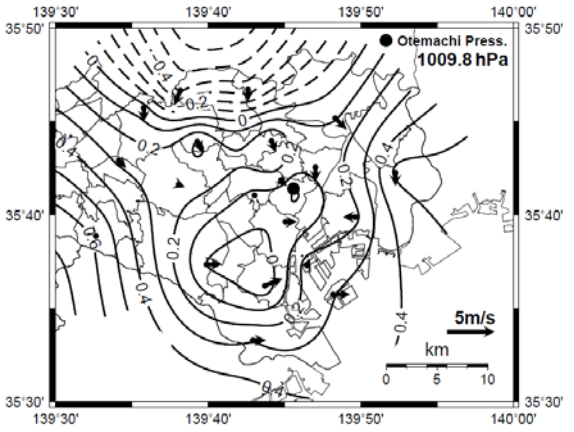

Fig. 4 A similar figure to Fig. 3, but at 07:00 JST July 8, 2004.

southerly geostrophic wind with a speed of the order of tens of ms^{-1}, light northerly winds were blowing at 07:00. Also, although the pressure patterns hardly changes between 02:00 and 07:00, the wind directions reverse at Stations 4 and 12. Moreover, the wind blows from the apparent low pressure area near Station 18 toward the eastern high pressure area, which is inconsistent.

A comparison of the atmospheric pressure at the three stations whose pressure values are representative of the METROS20 stations and the pressure at Otemachi is shown in Fig. 5 as time series during July 7 and July 8. July 7 was also a weak pressure gradient day (0.19 hPa/100 km). The pressure change at each station corresponds well to that at Otemachi, and in particular the pressure values at Station 10 (which is the nearest to Otemachi) are almost identical to those at Otemachi except during the period between 14:00 to 16:00 on both days. However, the values at Station 3 (or 12) are lower (or higher) than those at Otemachi throughout the two days. The characteristics of these

measured values at each station form the characteristic atmospheric pressure distribution pattern in the METROS20 seen in Fig. 3 and Fig. 4. Since the wind distribution does not correspond to the pressure distribution, it is thought that the data is affected by instrument errors at each station. The METROS20 wind vane and anemometer is a JMA's officially approved product, and is considered to be highly accurate.

On closer inspection of Fig. 5, the tendency for pressure values at Station 10 to be higher than those at Otemachi during the period from 14:00 to 16:00 on both days is also seen for Station 12. Kinetic wind pressure is one factor that can influence barometer measurements, and since it is proportional to the square of the wind speed, this influence becomes very strong when the wind speed is high (JMA 2002). The barometer at Otemachi is installed in an observation room, and is not likely to be affected by kinetic wind pressure. In comparison, since the METROS20 barometers were installed outside, they would be expected to be affected by kinetic wind pressure. For this reason, the barometer at Station 10 indicates a higher pressure than that at Otemachi when the sea breezes strengthen.

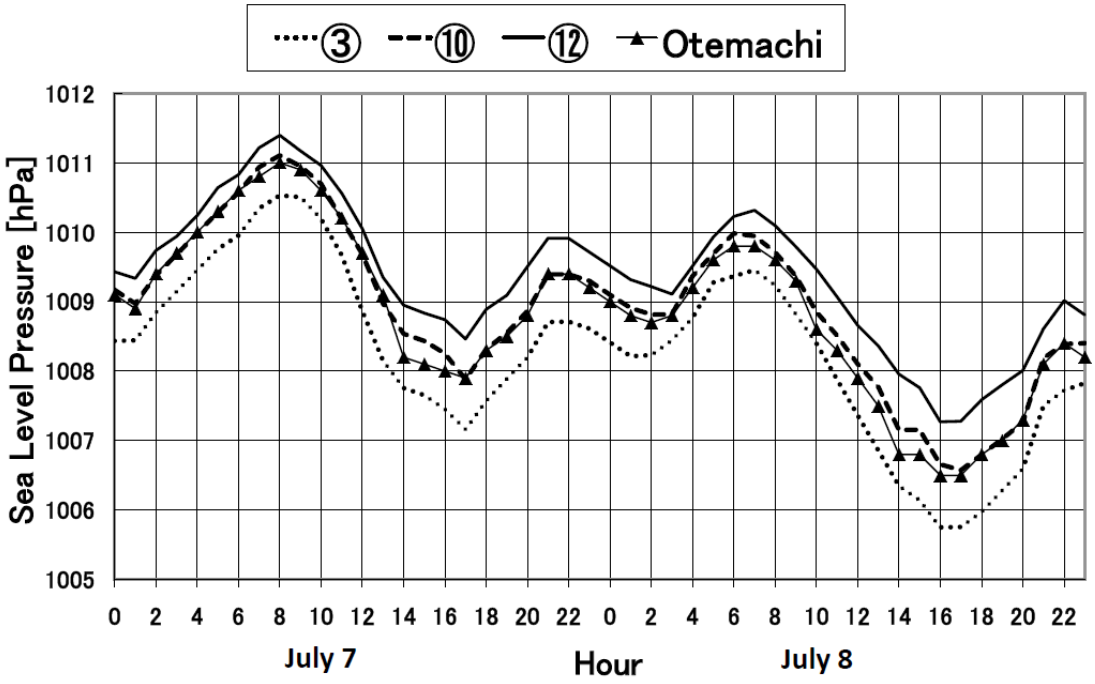

Fig. 5 Comparison of the sea level pressures at the three stations whose pressure values are representative of METROS20 stations and the pressure at Otemachi shown as a time series from July 7 to 8, 2004. The circled numbers in the legend on the top mean the station numbers of METROS20.

Figure 6 shows the relationship between the atmospheric pressure at Otemachi and that at Station 10, closest to Otemachi, at hourly intervals in July 2004. The relationship is seen to be highly linear, with a standard error of 0.13 hPa. The difference in spatial location between the stations and the above-mentioned influence of kinetic wind pressure are included in the standard error.

The standard error becomes 0.08 hPa during the period from 00:00 to 07:00, when the influence of kinetic wind pressure would be expected to be small, and the linear relationship is improved.

Therefore, data from this time period is suitable for correction of instrument errors in the METROS20 pressure data.

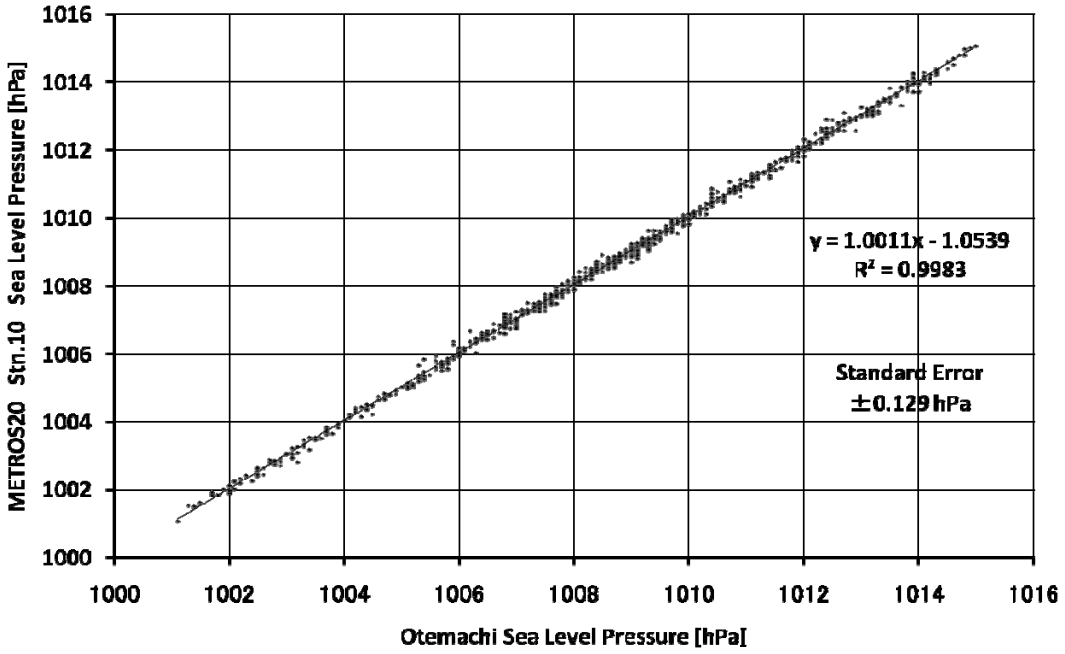

Fig. 6 Relationship between the sea level pressure at Otemachi and that at Station 10, which is the closest station to Otemachi, showing the observed value at hourly intervals in July 2004.

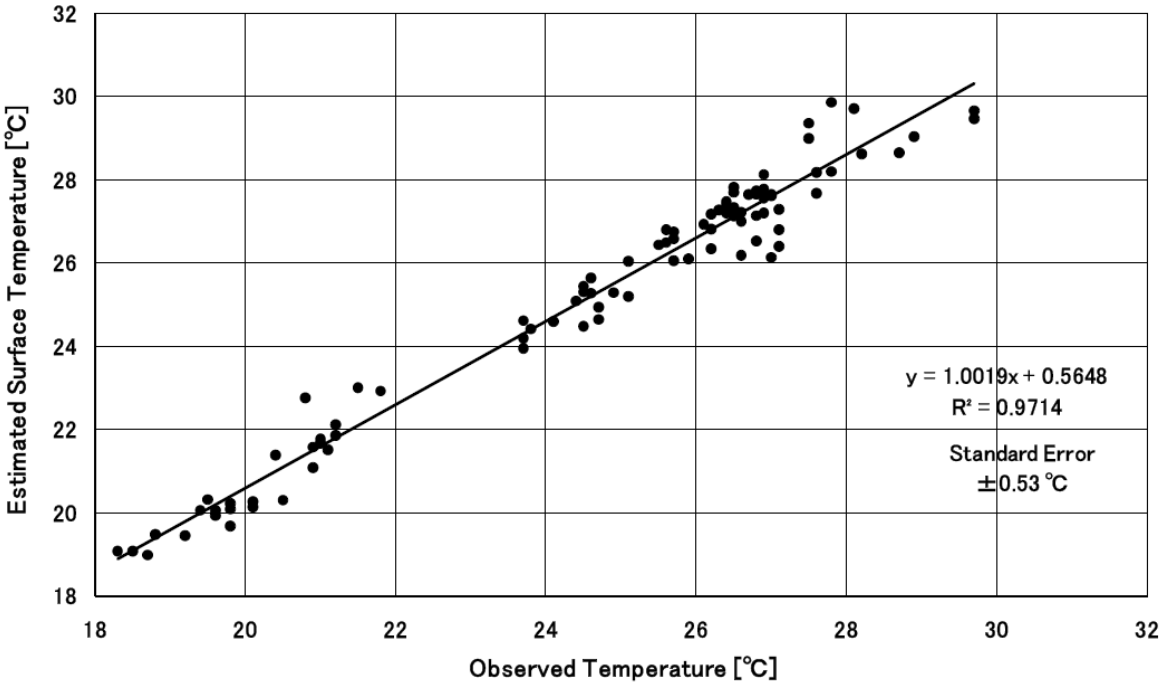

Fig. 7 Scatter diagram of the surface air temperatures estimated by interpolation of METROS100 temperature data plotted against the observed METROS20 temperatures at Station 4.

Estimation of surface air temperature and correction of pressure data

Figure 7 shows a scatter diagram of the surface air temperatures estimated by interpolation of METROS100 temperature data plotted against the observed METROS20 temperatures at Station 4. This figure consists of 96 data of 8 hours (00:00-07:00) for 12 weak pressure gradient days. The linear regression coefficient is close to 1.0, indicating a good correlation. The same analysis was repeated for all the METROS20 stations. At every station, the regression coefficient was close to 1.0 and the coefficient of determination was greater than 0.9. Therefore, the surface air temperatures can be estimated using these correlations. From Fig. 7, the estimated surface air temperature is about 0.6 °C higher than the observed temperature at Station 4, and this value corresponds to $c(n=4)$ in Fig. 2. The height at Station 4 is about 80 m. The temperature difference at every METROS20 station was similarly analyzed, and the corrected surface air temperatures were calculated.

Figure 8 shows a scatter diagram of the differences between the sea level pressures at Otemachi and those at Station 4 plotted against the differences between the temperatures at Otemachi and the corrected surface air temperatures at Station 4. This figure also consists of 96 data as the same as Fig. 7. It can be seen that the pressure at Otemachi is relatively low when the temperature at Otemachi is relatively high. This corresponds to a reversal of the signs of the temperature difference ΔT and the pressure difference Δp in Eq. (1). If we assume that hydrostatic equilibrium exists, the intercept on the vertical axis gives the pressure difference between the two barometers when the pressures at Otemachi and Station 4 are equal, because it corresponds to the point where no surface air temperature difference exists. The intercept on the vertical axis in Fig. 8 corresponds to $\Delta p(n=4)$ in Fig. 2. The negative value of $\Delta p(n=4)$, namely $-\Delta p(n=4)$ means the instrument error at Station 4 to Otemachi.

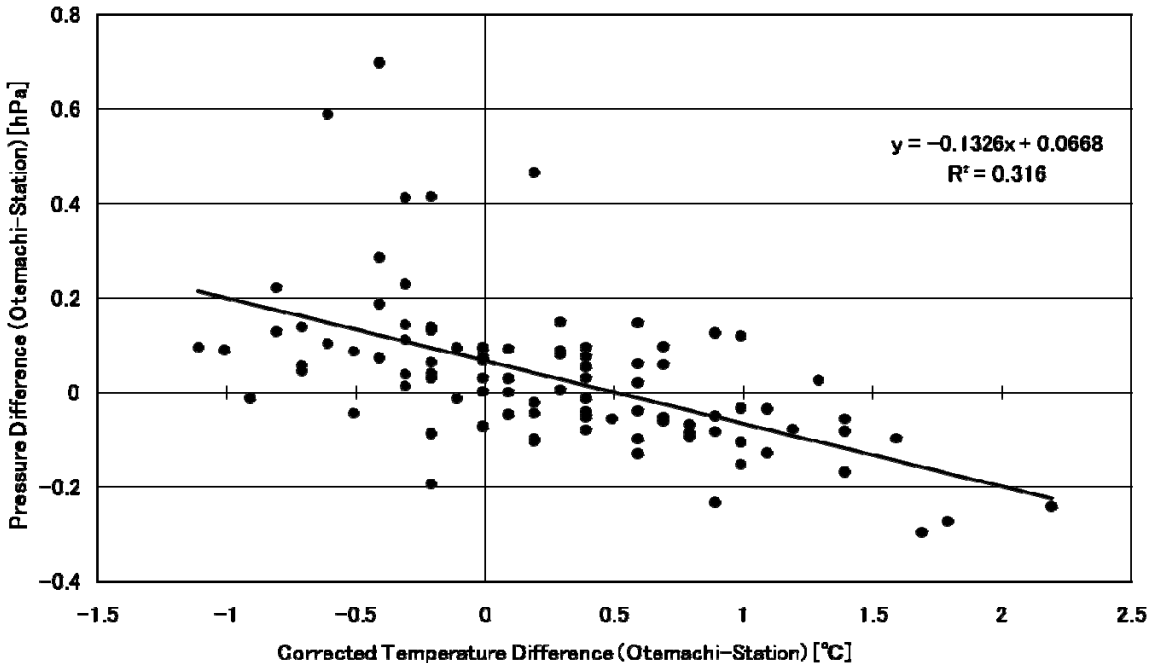

Fig. 8 Scatter diagram of the differences between the sea level pressures at Otemachi and those at Station 4 plotted against the differences between the temperatures at Otemachi and the corrected surface air temperatures at Station 4. The intercept on the vertical axis corresponds to $\Delta p(n=4)$ in Fig. 2.

Therefore, $\Delta p(n=4)$ means the correction value for the pressure data at Station 4. Station 4 was chosen, because it is relatively close to the center of Tokyo and the height of the urban boundary layer estimated from the value of $\Delta p/\Delta T$ is reflecting that over the center of Tokyo.

Figure 9 shows the intercept $\Delta p(n)$ and its 95% confidence interval at each METROS20 station. Although the pressure values at Stations 3 and 12 were lower and higher than those at Otemachi in Fig. 5, the higher and lower correction values at Stations 3 and 12 in Fig. 9 correspond to these deflections. Though positive and negative values of pressure difference exist, no dependence on the geographical distribution of stations can be seen. The 95% confidence interval has a minimum of 0.016 hPa at Station 10 in the central area, and a maximum of 0.069 hPa at Station 5 in the western area. From Fig. 9, the pressure difference between Otemachi and the METROS20 stations is largest about 0.53 hPa at Stations 2 and 3 in the northern area. There is a tendency for the 95% confidence interval to be larger in the peripheral areas of Tokyo. The corrected pressures are obtained by adding the central values in Fig. 9 to the uncorrected pressures.

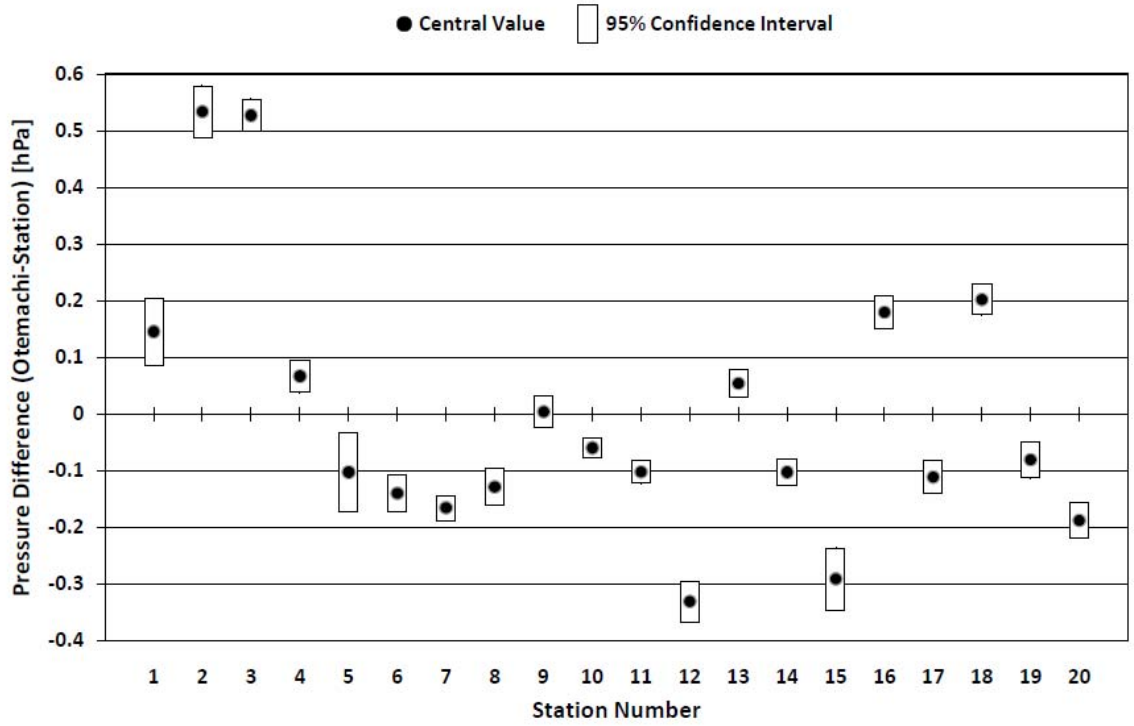

Fig. 9 Intercept $\Delta p(n)$ and its 95% confidence interval at each METROS20 station. $\Delta p(n)$ means the correction value for the pressure data at each station.

Evaluation of temperature and pressure differences

Here, we evaluate whether the relationship between the temperature and pressure differences shown in Fig. 8 is appropriate for the height of the urban boundary layer.

If we assume a uniform temperature difference up to the height of the urban boundary layer, Eq. (1) becomes as follows.

$$\Delta p = g\int_0^H \Delta\rho dz = -\frac{\rho_0 g}{T_0}\int_0^H \Delta T dz = -\frac{\rho_0 g \Delta T}{T_0} H \qquad (2)$$

The height of the urban boundary layer can be expressed as follows.

$$H = -\frac{T_0}{\rho_0 g}\frac{\Delta p}{\Delta T} \tag{3}$$

Using the values: standard temperature T_0 = 25 °C = 298 K, ρ_0 = 1.184 kgm^{-3} at this temperature, g = 9.81 ms^{-2}, and $\Delta p/\Delta T$ = -0.133 hPaK^{-1} (from Fig. 8), the height of the urban boundary layer becomes H = 340 m.

Fujibe (1987) calculated the height of the urban boundary layer at Otemachi in the daytime as 600 m using Δp = 0.05 hPa and ΔT = 0.2 °C. However, its height at nighttime is considerably lower because ΔT is nearly two times lower than in the daytime and Δp is hardly detectable.

From observations in Montreal, Oke (1993) found that the height of the urban boundary layer was about 300 m at the city center at nighttime. Moreover, the temperature was found to fall approximately linearly with height with a neutral or somewhat stable adiabatic lapse rate, and the temperature difference between the city and its surrounding areas disappears at the height of the urban boundary layer.

In Koganei City in Tokyo, Oda *et al.* (2010) determined the height of the urban boundary layer to be about 300 m from night to dawn using a ceilometer and an L-band wind profiler.

Thus, the height of the urban boundary layer estimated from Fig. 8 is largely in agreement with values found in previous studies and is considered to be appropriate.

Moreover, since the range of the values of $\Delta p/\Delta T$ at other observation stations except very close stations to Otemachi was -0.08 to -0.13 hPaK^{-1}, there is little problem in the assumption that the height of the urban boundary layer over the city is spatially uniform. The reason why the values of $\Delta p/\Delta T$ at very close stations to Otemachi become small is that both Δp and ΔT are very close to zero.

Pressure distribution using corrected pressure

As a case study of a typical heat island in the center of Tokyo, the surface air temperature distribution at 02:00 July 8, 2004, a weak pressure gradient day, is shown in Fig. 10. Also, the corrected pressure distribution is shown in Fig. 11. In Fig. 11, the characteristic pressure pattern seen in Fig. 3 and Fig. 4 does not appear, and the pressure gradients are small. A low pressure area surrounded by the 0.0 hPa isobar is observed on the northeastern side of Otemachi, with a pressure difference of 0.2-0.3 hPa compared to surrounding regions.

In Fig. 10, it can be seen that high temperature area surrounded by the +0.5 °C isotherm lies on the northeastern side of Otemachi, and it corresponds well to the low pressure area in Fig. 11. Also, at Stations 4 and 7, which have a temperature difference from Otemachi of about 0.0 °C, the pressure difference is 0.0 hPa, showing that the assumption of hydrostatic equilibrium holds. Moreover, the relationship between the temperature and pressure differences is as follows: at the western Station 5, the pressure difference is about +0.2 hPa with a temperature difference of -1.0 °C, and at the eastern Station 12, the pressure difference is about +0.2 hPa with a temperature difference of -1.5 °C. From these values, $\Delta p/\Delta T$ varies from -0.1 to -0.2 hPa°C $^{-1}$, and these values are consistent with the argument in the previous section.

In Fig. 11, the wind vectors in the coastal, southern, and northwestern areas show that the winds blow toward the center of Tokyo from the surrounding areas, and thus the wind system is consistent with the presence of a low pressure area. Although, the corrected pressure distribution at 07:00

July 8, 2004 (corresponding to Fig. 4) is omitted, the characteristics in the pressure and wind distributions shown in Fig. 11 are also seen.

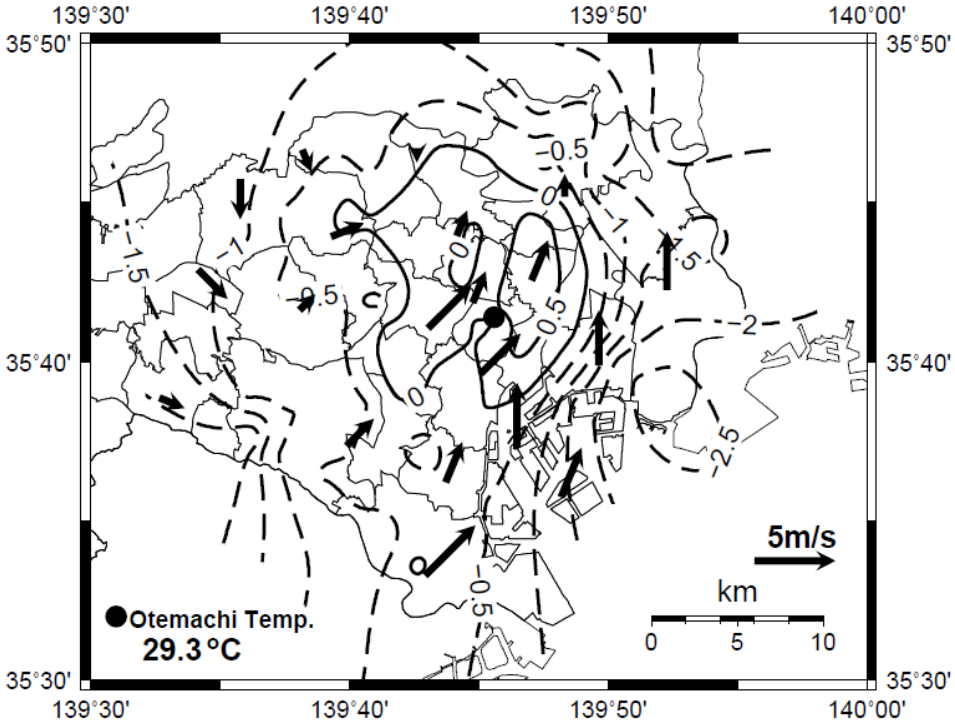

Fig. 10 Surface air temperature distribution (deviation from Otemachi) and wind vectors at 02:00 July 8, 2004.

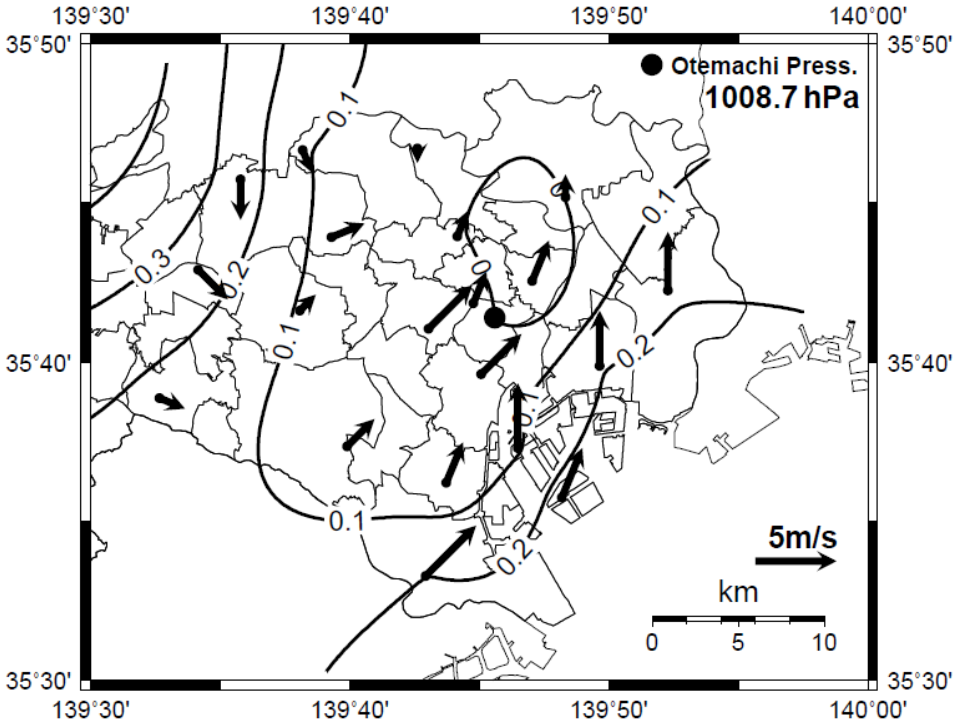

Fig. 11 Corrected sea level pressure distribution (deviation from Otemachi) of METROS20 and wind vectors at 02:00 July 8, 2004.

We calculated the magnitude of divergence and convergence in order to analyze the relationship between the wind system and the low pressure area in detail. The magnitude of divergence and convergence was calculated using Eq. (4), after the observed wind data were gridded and divided into *u*-components (E-W direction) and *v*-components (N-S direction).

$$D_{i,j} = \frac{\partial u}{\partial x} + \frac{\partial v}{\partial y} \cong \frac{1}{2}\left\{ \frac{u_{i+1,j} - u_{i-1,j}}{\Delta x} + \frac{v_{i,j+1} - v_{i,j-1}}{\Delta y} \right\} \quad (4)$$

Here, u and v are the E-W and N-S components of the wind velocity at each grid point, respectively, and i and j are the grid numbers in the E-W and N-S directions, respectively. Δx and Δy are the distances between grid points in the E-W and N-S directions, respectively. The intervals in the E-W and N-S directions were set at 1′15″ and 1′00″, respectively, so that Δx and Δy were almost equal (about 1.85 km). The observed wind velocity data were gridded by spatial interpolation using the surface algorithm of GMT4.3.1 (Wessel and Smith 1998).

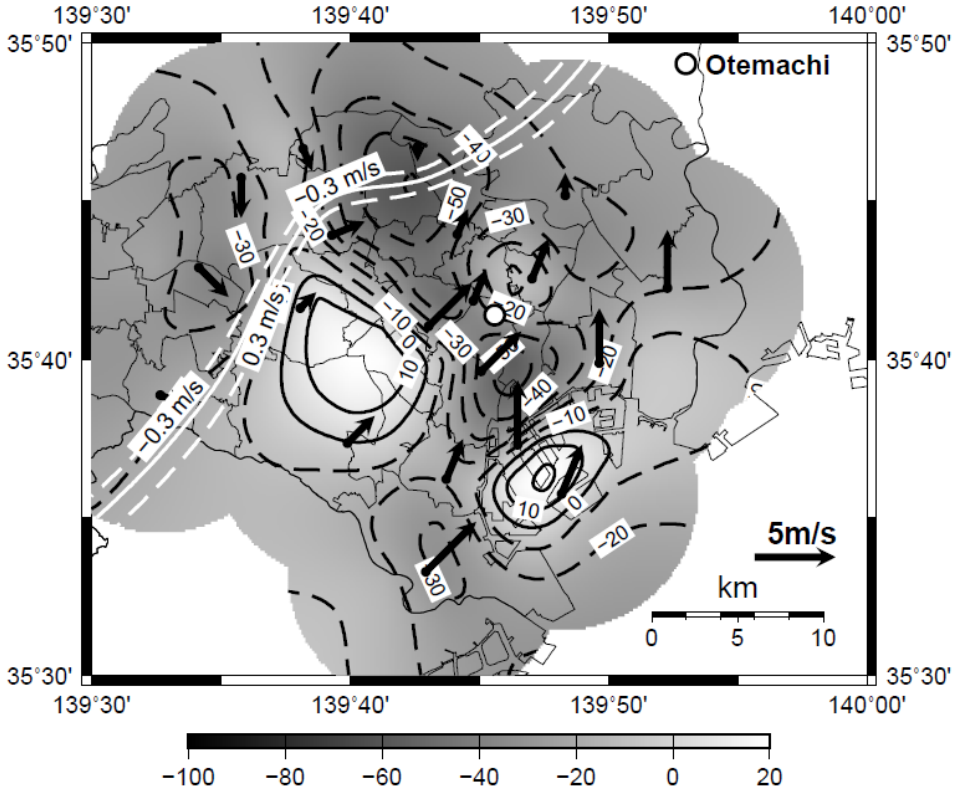

Fig. 12 The magnitude of divergence and convergence calculated by Eq. (4) and the N-S wind speed at 02:00 July 8, 2004. The magnitude of divergence (positive) and convergence (negative) is indicated by the gray scale at the bottom in the unit of 10^{-5} s^{-1}. The solid line (white) indicates the position where the N-S wind speed is 0.0 m/s, the broken lines (white) indicate ±0.3 m/s, with positive values corresponding to southerly winds.

The magnitude of divergence and convergence calculated by Eq. (4) and the N-S wind speed at 02:00 July 8, 2004 are shown in Fig. 12. The magnitude of divergence (positive) and convergence (negative) is indicated by the gray scale at the bottom in units of 10^{-5} s^{-1}. The solid line (white) indicates the position where the N-S wind speed is 0.0 m/s, the broken lines (white) indicate ±0.3 m/s, with positive values corresponding to southerly winds. Although local wind systems advance from the north (inland side) toward the south (sea side) during the nighttime, these are opposed by southerly winds. Moving from north to south across the boundary between these two wind patterns, the wind direction changes from northerly to southerly, and the N-S wind speed becomes 0.0 ms^{-1}. Therefore, the solid line (white) corresponds to the front of the local wind system, and hereafter the area between the broken lines is called as "the frontal zone." Convergence corresponding to the frontal zone is seen in the area among Stations 3, 6, and 7, and also near Station 13. The region to which these convergences are connected is located near Otemachi, and almost corresponds to the low pressure area of Fig. 11.

These results indicate that the effects of instrument error were successfully compensated for, because the corrected pressure distribution in Fig. 11 is consistent with the temperature, wind system, divergence distribution, and location of the frontal zone.

Figure 13 shows the atmospheric pressure difference between each METROS20 station and Otemachi, and the 95% and 99% confidence intervals of the corrected pressure at 02:00 July 8, 2004. Significant positive pressure differences are seen at almost all stations around the center of Tokyo, and a negative pressure difference is seen at Station 11. Such pressure distributions were found for many days when a typical UHI was formed. The pressure depression corresponding to high temperatures in

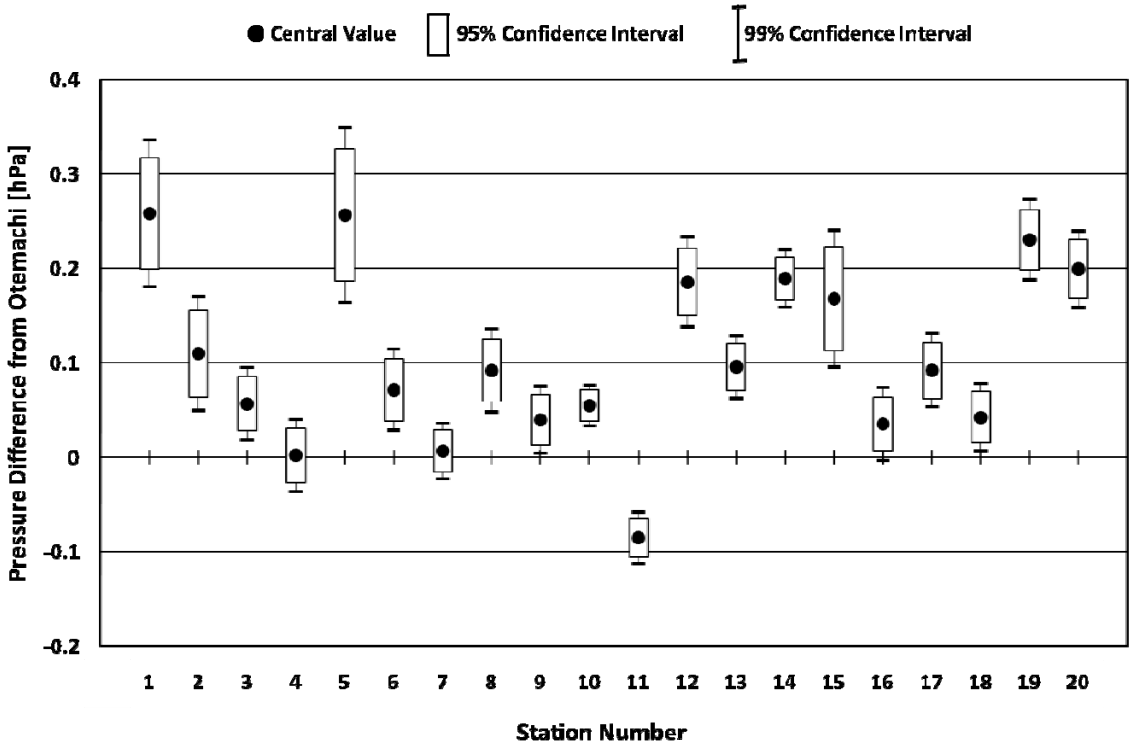

Fig. 13 Atmospheric pressure difference between each METROS20 station and Otemachi, and the 95% and 99% confidence intervals of the corrected pressure at 02:00 July 8, 2004.

the center of Tokyo is thus shown as a pressure distribution with significant pressure differences compared to the surrounding areas.

5. Conclusions

This study applied a correction to the METROS20 pressure data in order to compensate for instrument error by differences in measured pressure when the sea level pressure was actually same at Otemachi and each METROS20 station, by assuming hydrostatic equilibrium.

The corrected pressure distribution was found to be reasonable because it was spatially consistent with the air temperature distribution, wind system, and convergence zone. In a case study in which a typical urban heat island existed in the center of Tokyo, we detected a significant atmospheric pressure decrease of 0.2 or 0.3 hPa in the center of Tokyo compared to surrounding areas.

In this study, we calculated the value of the instrument error using the pressure data during the months of July and August, 2004, which was a hot summer. However, annual trends could be included in the METROS20 pressure data. Therefore, it is necessary to recalculate the instrument error values for other seasons and years.

Using the error correction method described in this paper, it became possible to determine the detailed pressure distribution in the Tokyo ward area for the first time, and to analyze the relationship between atmospheric pressure depression and high temperatures due to the UHI.

References

Bornstein, R. D. and Johnson, D. S. 1977. Urban-rural wind velocity differences. *Atmospheric Environment* **11**: 597-604.

Chandler, T. J. 1965. *The Climate of London*. London: Hutchinson.

Childs, P. P. and Raman, S. 2005. Observation and numerical simulations of urban heat island and sea breeze circulations over New York City. *Pure and Applied Geophysics* **162**: 1955-1980.

Fujibe, F. 1987. Weekday-weekend differences of urban climates, part 1: Temporal variation of air temperature and other meteorological parameters in the central part of Tokyo. *Journal of the Meteorological Society of Japan* **65**: 923-929.

Fujibe, F. 1988. Weekday-weekend differences of urban climates, part 3: Temperature and wind fields around Tokyo and Osaka. *Journal of the Meteorological Society of Japan* **66**: 377-385.

Fujibe, F. 1994. Long-term falling trends of pressure over the Kanto Plain as evidence of increasing heat content in the lower atmosphere in the daytime of the warm season. *Journal of the Meteorological Society of Japan* **72**: 785-792.

Fujibe, F. 2003. Long-term surface wind changes in the Tokyo metropolitan area in the afternoon of sunny days in the warm season. *Journal of the Meteorological Society of Japan* **81**: 141-149.

Fujibe, F. and Asai, T. 1980. Some features of a surface wind system associated with the Tokyo heat island. *Journal of the Meteorological Society of Japan* **58**: 149-152.

JMA. 2002. *Guideline for Surface Meteorology Observation.* Tokyo: Japan Meteorological Agency, 19-32*.

Landsberg, H. E. 1981. *The Urban Climate*. New York: Academic Press.
MSJ (Meteorological Society of Japan). 2003. Climate information. *Tenki* **50**: 734, 812*.
MSJ (Meteorological Society of Japan). 2004. Climate information. *Tenki* **51**: 693, 749*.
Mikami, T. 2006. Recent progress in urban heat island studies: Focusing on the case studies in Tokyo. *E-Journal GEO* **1**: 79-88**.
Nishina, J. and Mikami, T. 2008. Diurnal variation of the local air-pressure system in the urban Tokyo on summer calm days. *Quarterly Journal of Geography* **60**: 121-130**.
Oda, R., Iwai, H., Ono, Y., Kawamura, S., Sekizawa, S., Ishii, M., Mizutani, K. and Murayama, Y. 2010. Estimation of diurnal variation of urban boundary layer over Koganei City in Tokyo. *Abstracts of the Meteorological Society of Japan 2010 Spring Meeting* **97**: 314*.
Oke, T. R. 1987. *Boundary Layer Climates*. *Second Edition*. London: Routledge.
Oke, T. R. 1993. The heat island of the urban boundary layer. Characteristics, causes and effects. In *Wind Climate in Cities*. Ed. Cermak, J. E., Davenport, A. G., Plate, E. J. and Viegas, D. X., 81-108. Dordrecht: Kluwer Academic Publishers.
Okita, T. 1960. Estimation of direction of air flow from observation of rime ice. *Journal of the Meteorological Society of Japan* **38**: 207-209.
Sawada, Y. and Takahashi, H. 2007. Relationship between the intensity of convective rainfall in central Tokyo and the distribution of surface temperature and wind systems over the Kanto plain in summer. *Geographical Review of Japan* **80**: 70-86**.
Shreffler, J.H. 1978. Detection of centripetal heat-island circulations from tower data in St. Louis. *Boundary-Layer Meteorology* **15**: 229-242.
Shreffler, J.H. 1979. Heat island convergence in St. Louis during calm periods. *Journal of Applied Meteorology* **18**: 1512-1520.
Takahashi, H. 1998. Climatological feature of diurnal variation in wind systems and divergence field over Kanto district under stable synoptic conditions: In the cases of summertime land-sea breezes and strong winter monsoon. *The New Geography* **45**: 34-53**.
Wessel, P. and Smith, W.H.F. 1998. New, improved version of Generic Mapping Tools released. *Eos, Transactions, American Geophysical Union* **79**: 579.

(*: in Japanese, **: in Japanese with English abstract)